Research Article

Frederico Lima, Isman Khazi*, Ulrich Mescheder, Alok C. Tungal and Uma Muthiah

Fabrication of 3D microstructures using grayscale lithography

Abstract: Following the demand for three-dimensional (3D) micromachined structures, additive and subtractive processes were developed for fabrication of real 3D shapes in metals, alloys and monocrystalline Si (c-Si). As a primary structuring step for well-defined 3D structuring of the photoresist, grayscale lithography by laser direct writing was used. For additive fabrication of 3D microstructures, structured photoresist was used as molds. They were sputtered and subsequently electroplated by a metal (Cu) and an alloy (NiCo). The derived electroplated structures were demolded from the photoresist using an organic stripper. These metal structures are satisfactory replicas of the photoresist pattern. For subtractive pattern transfer of 3D structures into c-Si, reactive ion etching (RIE) was used to transfer the 3D photoresist structure into c-Si with 1:1 pattern transferability. The process parameters of RIE were optimized to obtain a selectivity of 1 and an anisotropy factor close to 1. Whereas conventional X-ray lithography (LIGA) and nanoimprint lithography result in 2.5D patterns, these techniques allow the fabrication of almost any arbitrary 3D shapes with high accuracy. In many cases, 3D structures ('free forms') are required, e.g. for molding of optical components such as spheres (or aspheres), channels for lab-on-a-chip and pillars for biological applications. Moreover, 3D structures on Si could be used as optical gratings and sensors.

1 Introduction

The fabrication of complex three-dimensional (3D) structures in the micrometer range is usually limited by the processes available. Especially, the standard subtractive structuring process used in microtechnology provides only 2D structures due to limitations in normal photolithography (limited depth of focus and small photoresist thickness), thin film deposition techniques (typical thickness less than 1 μm) and transfer process via physical and/or chemical etching. Bulk micromachining using anisotropic electrochemical etching of c-Si provides 3D structures. However, the shapes of these structures are restricted to specific crystal planes, e.g. the (111) planes. Molding of metals into deep photoresist patterns with vertical sidewalls derived either by X-ray lithography (LIGA) [1] or standard photolithography using SU-8 [2] provides only 2.5D structures, i.e. structures with vertical sidewalls and constant structure width over the full depth of the structure. A further option is the usage of nanoimprint lithography, but it allows the generation of 3D structures only at some specific boundary conditions [3]. However, such structures do not fulfill the requirements of several applications: microlens arrays for optoelectronic devices [4–6], diffractive gratings [7, 8], thin film transistors [9], very complex micro- and nanofluidic devices [10, 11] and micro-helices [12]. Therefore, several research groups have been investigating processes which allow 3D microstructuring [13–15]. An example is the use of diffraction from an excimer laser system to obtain conical, trihedral and pyramidal 3D structures [16]. The problem is that the machining principle does not allow very precise

*Corresponding author: Isman Khazi, Institute for Microsystems Technology (iMST), Faculty of Mechanical and Medical Engineering, Furtwangen University, Robert-Gerwig-Platz 1, 78120 Furtwangen, Germany; and Department of Microsystems Engineering (IMTEK), University of Freiburg, Freiburg im Breisgau, Germany, e-mail: kmi@hs-furtwangen.de. https://orcid.org/0000-0001-7721-6916
Frederico Lima: Institute for Microsystems Technology (iMST), Faculty of Mechanical and Medical Engineering, Furtwangen University, Robert-Gerwig-Platz 1, 78120 Furtwangen, Germany; and Department of Microsystems Engineering (IMTEK), University of Freiburg, Freiburg im Breisgau, Germany
Ulrich Mescheder: Institute for Microsystems Technology (iMST), Faculty of Mechanical and Medical Engineering, Furtwangen University, Robert-Gerwig-Platz 1, 78120 Furtwangen, Germany
Alok C. Tungal: Nanoscribe GmbH, Hermann-von-Helmholtz-Platz 1, 76344 Eggenstein-Leopoldshafen, Germany
Uma Muthiah: AKKA GmbH & Co. KGaA, Neugablonzer Str. 13, 93073 Neutraubling, Germany

fabrication of sharp profiles (i.e. points, corners and edges). The same type of laser has also been used for the manufacturing of hexagonal arrays [17]. In this case, areas far away from the structure center had larger discrepancies than the expected geometry. Another approach is to use thermal reflow process to obtain the desired shapes such as 3D photoresist structures for optical lens application [18]. However, the accuracy of the resulting 3D geometry is very difficult to control; it strongly depends on hard bake duration and temperature. Furthermore, grayscale lithography is reported to realize 3D photoresist structures, wherein the exposure dose is modulated in the depth of the photoresist, thereby resulting in 3D structures after development. Grayscale masks can be used to reach different local exposure intensities for photoresist structuring, which is, however, a tedious job [13]. Additionally, laser direct writing lithography (DWL) systems are well appropriated for such processes due to their accuracy, flexibility and capability of generating complex structures within thick resist layers. Such systems normally consist of an XY stage which moves during the process and a fixed optical unit responsible for the exposure of the sample with a desired pattern [15]. Furthermore, this process is not limited to a single photoresist, but it can be used for any photoresist. Therefore, a calibration of depth as a function of laser dose is required for new combinations of photoresists and processes (i.e. spinning and hardening process parameters).

In this research, a DWL system was used to produce 3D photoresist structures with a very simple method: varying the intensity of the laser writing source during exposure. Exposed and developed photoresist structures were transferred using additive and subtractive approaches. The former was done by the microelectroplating of Cu and NiCo alloys, thereby resulting in 3D metal free forms. On the other hand, the latter was realized using reactive ion etching (RIE) with an optimized process with a selectivity of 1 and an anisotropy close to 1, enabling a 1:1 pattern transfer of the structured photoresist to the Si substrate with high dimensional accuracy and with high surface quality (i.e. low surface roughness) of the etched structures.

2 Experimental

In this work, the AZ 4562 (positive photoresist) and AZ 351B (developer) (both from Microchemicals GmbH, Ulm, Germany) were used for both additive and subtractive pattern transfer of 3D photoresist structures. A total thickness of 8 μm was defined by conventional resist spinning at 2800 rpm for 30 s and acceleration of 2000 rpm/s. Prior to photoresist coating, Ti Prime adhesive coating (Microchemicals GmbH, Ulm, Germany) was spin coated at a speed of 4000 rpm for 20 s and an acceleration of 2500 rpm/s. Grayscale lithography

was realized by a laser direct writing system (DWL 66FS, Heildelberg Instruments Mikrotechnik GmbH, Heidelberg, Germany). The system allows photoresist exposure with up to 128 grayscales, a lateral resolution of 0.6 μm and an alignment accuracy of 200 nm (3σ) [19]. The optical setup uses a blue diode laser with a wavelength of 405 nm. The development of the exposed photoresist was done using a rocking table of type REAX3 (Heidolph Instruments GmbH & CO., Schwabach, Bayern, Germany) for 3.75 min. The developer was diluted in a volumetric ratio of four parts of water and one part of AZ 351B. After development, the samples were hard baked using a hotplate or an oven.

For the additive pattern transfer, concave and convex structures were fabricated. Pd (100 nm) was sputtered on the 3D patterned (convex and concave) photoresist using a sputter coater Bal-Tec SCD 004 (BAL-TEC AG, Balzers, Liechtenstein) with a current of 60 mA for 120 s. This Pd layer provided the plating base for the later electroplating process. The samples were placed at a distance of 5 cm from the target in a vacuum of 5×10^{-2} mbar, and Argon plasma was used. A process trade-off is the formation of cracks in the Pd plating base on the 3D photoresist patterns. Therefore, an optimization of the hard baking conditions was required to reach a plating base with neither defects nor deformation of the structure geometry. 3D patterned photoresist structures were deposited by thick metal layers during the electrochemical deposition processes. A mechanically hard NiCo alloy [20] and Cu were selected for the additive pattern transfer. NiCo alloys can be used to fabricate ferromagnetic devices, while Cu has great electrical properties. Microelectroplating processes were realized with a Biologic SP-150 potentiostat (Bio-Logic Science Instruments, Seyssinet-Pariset, France). Cu deposition was done in a glass beaker using an acidic copper sulfate electrolyte (CupraBase50) from Atotech Deutschland GmbH (Berlin, Germany). A soluble Cu counter electrode was used to avoid an ionic metal concentration drop in the solution during electroplating and a self-made holder with an opening of 0.5 cm² for the working electrode. Electrochemical measurements were done using the counter electrode as a reference. The distance between electrodes was around 5 cm. NiCo alloy microelectroplating was carried out using a bath consisting of sulfamate salts of Ni and Co. Boric acid and nickel chloride were used as a buffering agent and to avoid passivation of the Ni anode, respectively. In addition, saccharin was added to the electrolyte to coat stress-free deposits, and sodium lauryl sulfate was used as an anti-pitting agent to ease the hydrogen evolution during cathodic reduction in order to produce smooth polished electrodeposits in the case of NiCo. All the chemicals for the NiCo electrolyte were purchased from Subolab GmbH (Pfinztal, Germany). The electrolyte was prepared to obtain an alloy with a ratio of 30 wt% Co and 70 wt% Ni. This alloy combination shows better magnetic and mechanical properties (microhardness ca. 600 HV1). A 400-ml three-electrode electrolytic cell was used for deposition processes. The counter and reference electrodes were 99% pure Ni plate (800 μm thick, 3 cm²) and Ag/AgCl in 3 м KCl, respectively. The electrolyte composition and operating parameters are described in [20]. The desired thickness was pre-calculated using Faraday's law of electrolysis. For all the experiments (Cu and NiCo), a magnet stirrer was used to keep a homogeneous ionic metal concentration in the bath. The separation process of the electroplated metal from the photoresist mold was done by dipping the probe into an inorganic stripper, Micro D350 (DMSO) from Microchemicals GmbH (Ulm, Germany) using ultrasound.

Subtractive patterns into c-Si were realized by an optimized RIE in Plasmalab 100 (Oxford Instruments, Yatton, Bristol, UK) with a selectivity of 1 and an anisotropy factor close to 1. The process settings were temperature of 10°C, pressure of 10 mTorr, radio frequency (RF)

power of 100 W and flows of 3 sccm for SF_6 and 35 sccm for CHF_3, as described in detail in [19]. An array of 3D micropyramids with different heights (2–8 µm in steps of 1-µm height increment) were exposed in AZ4562 and transferred into c-Si by RIE with selectivity of 1:1.

The 3D patterns were characterized by a scanning electron microscope (SEM) (JEOL 5400, Jeol Ltd., Akishima, Tokyo, Japan), a white light interferometer (Zygo's NewView™ 7100, Zygo Corporation, Middlefield, CT, USA) and a profilometer (Dektak 150 from Veeco Instruments Inc., Plainview, NY, USA), and the surface quality by an Autoprobe CP atomic force microscope (AFM) from Park Scientific Instruments (Sunnyvale, CA, USA).

3 Concept of the 3D micropattern transfer using grayscale lithography

3.1 Principle of grayscale lithography

Grayscale lithography using the DWL 66FS from Heidelberg Instruments exploits the ability of modulating the intensity of the laser source, which is used for the mask manufacturing and the maskless direct writing on the wafer. On contrary to conventional lithography, which is binary in nature (i.e. after development, the exposed resist is completely removed at the exposed areas in case of a positive resist), grayscale lithography using direct writing operates with continuous variation of the laser intensity. The laser penetrates the photoresist with different depths, thereby enabling the exposure of any arbitrary real 3D shapes. Figure 1 shows the principle of grayscale lithography, wherein the thick positive photoresist that coats the Si wafer is exposed with variable laser intensities, resulting in the 3D exposure of the photoresist after development as shown by the dark red region, while the light red region is fully exposed until the base of the photoresist, which is removed during the development. The variable laser intensities of the DWL are associated with the so-called 'gray values'; the smaller this value is, the lower the laser intensity is, and vice versa. In Figure 1, the blocks of rectangles above the photoresist represent the CAD mask design. Each rectangle is assigned with a specific gray value, and hence, a specific dose is exposed in the photoresist as shown by the length of the arrows; wherein, the longest arrow refers to the dose to clear. In this schematic representation, the center square block is assigned the least gray value. Therefore, the photoresist is exposed with the least laser intensity in the middle square, and the specific dose increases moving further away from the center square, thereby resulting in a controlled gradient in the exposure profile, which consecutively results in the 3D exposure of the photoresist as shown by the dark red region in Figure 1.

Contrary to the conventional 2D lithography, wherein the CAD mask design for the single exposure is designed in a single layer, in the case of the grayscale exposures, the CAD mask design must be designed in multiple layers considering the required 3D photoresist profile. For example, in Figure 1, the CAD mask design shows different blocks of rectangles with varying colors, wherein the blocks of rectangles with a similar color are designed in the same layer of the CAD software. Furthermore, in the user interface of the DWL 66FS, the layers of the CAD mask design are assigned to a particular gray value considering the required dose of exposure to realize the required 3D profile in the photoresist. The blocks of rectangles within
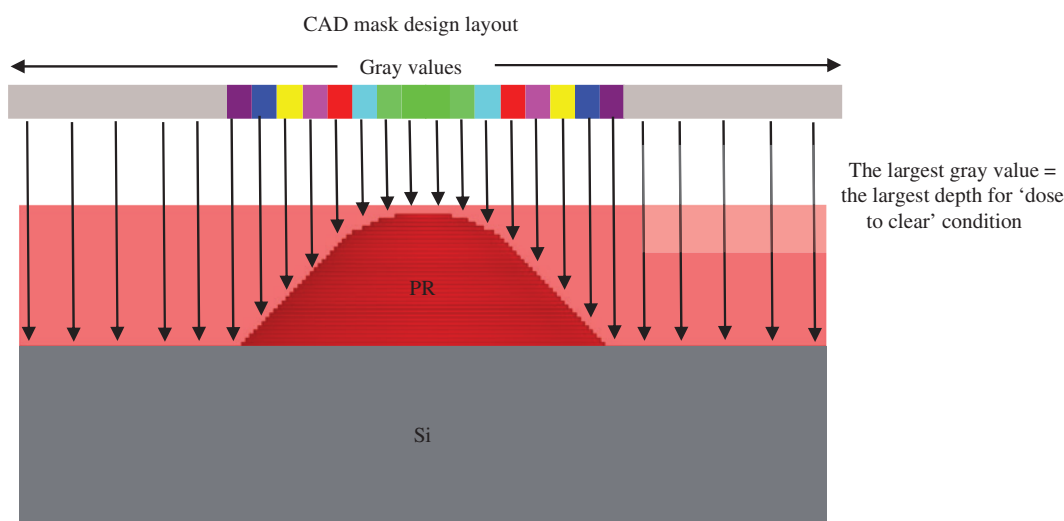
Figure 1: Schematic showing the concept of gray scale lithography using direct writing laser.

similar layers are exposed with a single gray value. Therefore, any arbitrary 3D profile geometry can be exposed by an appropriate CAD mask design and the association of the gray values with the layers in the CAD mask design in the exposure software of the DWL 66FS tool. The user interface of the DWL 66FS provides the modulation of 128 gray values for a one-time exposure. However, up to 12 times exposures are possible; thereby, much more than 128 gray values can be, in principle, obtained, i.e. a very smooth gradient in the 3D profile can be realized. The relation of the gray value numbers with the respective dose to clear is obtained by the grayscale calibration curve, which is specific to a given photoresist with respective processing conditions. The intensity and the focus of the laser are fixed, and the photoresist is exposed with variable gray values. In this work, the calibration curve is obtained by the exposure of AZ4562 photoresist with 32 well-separated rectangles, wherein each rectangle is exposed with a specific gray value for a fixed laser intensity and focus. The CAD mask design for this exposure had 32 layers with an array of rectangles, wherein each rectangle was assigned with an individual layer, respectively. Ensuing, the layers were associated with respective gray values from 0 to 127 (in steps of 4) and were exposed in the 8-μm-thick AZ4562 photoresist. Subsequently, it was developed, and the exposed profile was characterized to measure the depth of exposure in the photoresist by a profilometer as shown in Figure 2A. The depth of exposure increases with gray values, which can be seen by a stepwise transition in the depth of the photoresist, with complete exposure of the photoresist at the highest gray value of 127. Figure 2B represents the calibration curve, wherein the gray values are related with the measured depth of exposure from Figure 2A. Moreover, the obtained exposure depths for the respective gray values are fitted by a second-degree polynomial curve to obtain the respective polynomial equation as shown in Figure 2A. Therefore, with the help of the obtained calibration equation, gray values for any required depth of exposure can be obtained, and hence, any arbitrary 3D microstructure can be easily exposed using this method. Furthermore, it can be observed from the curves in Figure 2A and B that at lower exposure depth, there is an abrupt transition in the depth with respect to the gray values. This effect can be attributed to the inhomogeneity in the thick photoresist profile; however, it can be optimized by decreasing the gray value step size to get a more accurate calibration curve. Finally, the pattern transfer of the 3D structured photoresist into c-Si is done by subtractive fabrication using a special RIE process [19], whereas for metals and alloys, the transfer process is realized using additive fabrication by microelectroplating as shown in Figure 3. The exact replica of the 3D structured photoresist is obtained in c-Si by subtractive fabrication, while its negative replica is obtained in metal and alloys by additive fabrication using microelectroplating.

3.2 Principle of the subtractive pattern transfer by RIE

The combination of grayscale lithography with RIE for subtractive pattern transfer is referred to as grayscale technology [21]. The 3D photoresist profile can be transferred into c-Si by RIE within a process window which results in a selectivity (S) exactly equal to 1 (i.e. same
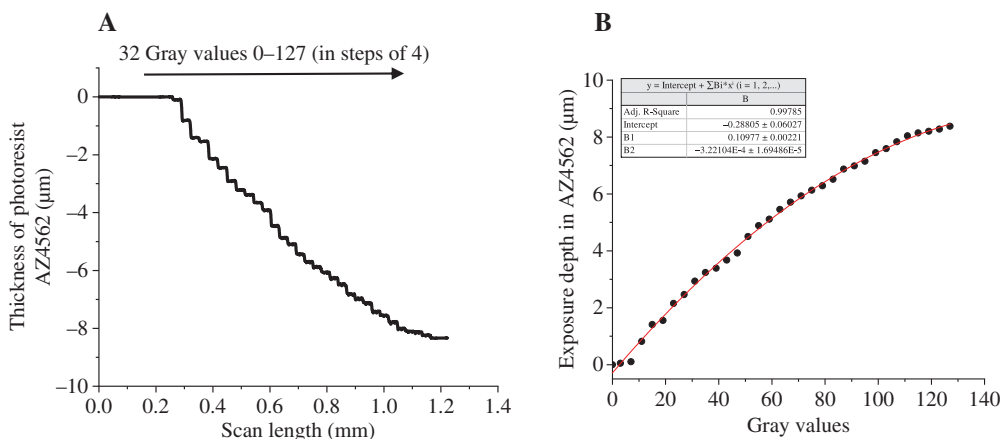
Figure 2: Calibration curve of the direct writing system for the AZ 4562 (positive resist) and AZ 351B (developer). (A) Measured thickness of the photoresist AZ4562 after exposure and development with 32 different gray values from 0 to 127 in steps of the 4. (B) The calibration curve relating the gray values with their respective exposure depths.

Figure 3: Pattern transfer in Si by subtractive fabrication and in metal and alloys by additive fabrication, schematics (A) a patterned photoresist, (B) transferred into c-Si by RIE, (C) transferred to a metal by means of electroplating.

etch rates in the photoresist as well as the c-Si) and an anisotropy factor ($A_f = 1$ − lateral etch rate/vertical etch rate) close to 1; the importance of this fundamental requirement for accurate pattern transfer and the optimization of RIE parameters has already been explained in detail [21]. The RIE process parameters include etchant gas flow rate (in this study: SF_6), passivation gas flow rate (in this study: CHF_3), RF power, pressure and temperature, which can be adjusted to attain $S = 1$ and anisotropy factor close to 1. Furthermore, the anisotropic profile can be adjusted by controlling the CHF_3 flow rate, which partially passivates the surface, thereby hindering the lateral etching in both the photoresist and the c-Si substrate. The principle of the 1:1 pattern transfer is depicted schematically in a cross-sectional view in Figure 4A–E, wherein a 3D structured photoresist in the form of a triangle using grayscale lithography is shown on the c-Si substrate. Figure 4A shows the direction of etching (represented by arrows) of the Si atoms from the photoresist-free regions on the c-Si wafer and the photoresist by RIE. At the point in time when the

Figure 4: Concept of subtractive pattern transfer using RIE with $S = 1$ and $A_f = 1$, (A) Si and PR atoms are etched away, (B) profile gradient is formed, (C) etching continues with well-maintained gradient in profile, (D) $A_f = 1$, no lateral etching, (E) pattern transferred 1:1 into c-Si.

thinnest photoresist is etched away completely, the open c-Si surface around it is already etched away, thereby resulting in a profile gradient between them as shown in Figure 4B. For $A_f = 1$, the etching is strictly in the vertical direction; thereby, the gradient in the profile (between the Si surface and the etched structure) is well persevered during the etching because of the uniform removal of Si atoms and photoresist atoms (i.e. $S = 1$), consecutively resulting in the well preservation of the geometric profile of the 3D structured photoresist during the pattern transfer as shown in Figure 4C–E. Subsequently, the pattern is successfully transferred 1:1 from the structured photoresist to the c-Si wafer. Therefore, the resulting pattern is an exact replica of the 3D structured photoresist profile in the c-Si wafer for the given conditions of $S = 1$ and $A_f \approx 1$.

3.3 Principle of the additive pattern transfer by microelectroplating

The 3D structured photoresist was coated by a thin conductive seed layer (plating base) usually 50–100 nm thick as shown in Figure 3C. Microelectroplating was used to deposit metals or alloys onto/into the 3D structured photoresist, owing to its ability to deposit thick stress-free structures [22]. Different to the LIGA technique, in this technique, the seed layer is coated after the 3D structuring of the photoresist. After deposition, the photoresist mold is removed by dissolution in a suitable liquid organic stripper, or, depending on the structure geometry, it can be physically peeled off from the mold. Furthermore, the obtained microstructure is a negative replica of the 3D structured photoresist pattern using grayscale lithography as shown in Figure 3B.

4 Results and discussion

For the fabrication of the 3D structures, the calibration curve from Figure 2B was used to obtain the required gray values for the respective grayscale exposures for the additive (i.e. convex and concave lenses) and subtractive fabrication (3D micropyramids) in this work. The resulting equation of the second-order polynomial fit from Figure 2B is shown in Equation (1), which was used to compute the gray values for the exposures in this work.

$$y = 0.1097\ \mu m\ x^2 - 0.00032\ \mu m\ x - 0.288\ \mu m \qquad (1)$$

where x is the grayscale value.

4.1 Additive fabrication of the 3D free forms

4.1.1 Photoresist structuring, plating base deposition and microelectroplating

Convex and concave 3D microstructures were exposed using grayscale lithography having a diameter of 600 μm, with 4- to 5-μm height and depth, respectively. The patterned photoresist structures were initially hard baked using a hotplate at a temperature of 120°C for 2 min. However, as the change from Pd to Pt did not show any reduction in crack formation, we suppose that the crack formation is mainly a result of the different thermal expansion coefficients of the photoresist and metal film. Moreover, the role of photoresist processing, especially hard baking, was investigated in detail to avoid cracks.

Hard baking using a hotplate was determined as inappropriate for such a process due to an inhomogeneous heat gradient in the photoresist. This behavior is addressed in the evaporation of solvent, limiting the photoresist to reach a minimum required stability. Therefore, cracks were observed through the sputtered Pd layer. To avoid this problem, the hotplate was replaced by an oven for hard baking. The latter can offer a more gentle temperature increase during heating and a more homogeneous temperature gradient and, consequently, an appropriate evaporation of the photoresist solvent. Following the post process steps, no cracks were observed on the sputtered Pd layer. However, a critical process window must be considered within which crack formation can be neglected. A small change in time, temperature and room environment can cause deformation of the photoresist patterns or cracks. Such morphology dependence on the baking process is exemplified in Table 1, showing an optimal process window at baking temperature of 125°C and a hard baking time of 28 min.

Even before sputtering, shape deformation of the resist pattern can be easily observed. This effect was quantified using measurements with a white light interferometer.

Table 1: Influence of hard baking parameters in an oven on Pd sputtered layer and patterned photoresist.

Hard bake temperature (°C)	Hard back time (min)	Observed morphology
100	4	Surface with minor wrinkles
100	60	Surface predominantly wrinkled
120	30	Minor cracks, structure deformation
122	28	Small cracks all over the area
125	28	No cracks, neither deformation
130	22	No cracks, structure deformation

Measurements done prior and after hard baking for the two cases listed in Table 1 are displayed in Figure 5. Patterned photoresist structure deformations were observed already after hard baking for the following experiments: 100°C for 60 min, 120°C with duration of 30 min and 130°C for 22 min. For lower temperatures, wrinkled surfaces were observed after sputtering. During sputtering, the photoresist suffered a volume increase. Afterward, it decreased, causing the sputtered layer to obtain a wrinkled surface. This suggests that the photoresist did not harden enough to support the sputtering conditions. On the other hand, cracks were formed during Pd sputtering for samples hard baked at temperatures of 120°C and 122°C for 30 and 28 min, respectively. For higher temperatures, the time can be reduced, but the structure still suffers from deformation, though cracks are not further observed. The SEM micrographs of these samples are shown in Figure 6. We conclude that for the used AZ 4562, only a tight process window exists in which both crack formation and pattern deformation can be avoided. Similar photoresist deformations have been reported, and the cause was stated to be the dominance of the resist crosslink reactions over surface tensions during hard baking [23, 24]. This explanation fits well for the cases shown in this work.

Cu microelectroplating was done using a fixed current density of 60 mA/cm² for 45 min. Such parameters were determined to reach a layer thickness of 60 μm. Images of a patterned photoresist and its final demolded Cu structure can be seen in Figure 7. NiCo microelectroplating was carried out galvanostatically with a low current density (10 mA/cm²) for 5 h. This helps achieve a uniform deposition onto the 3D photoresist mold.

4.1.2 Transfer characterization

The transfer quality was characterized using cross sections from the center of the structures. They were obtained from white light interferometer 3D measurements (see Figure 7) and compared after development, hard baking, sputtering and for the demolded metal structure (see Figure 8A). The demolded Cu structure measurements were inverted to allow an easier comparison. For an optimal hard bake process ($T = 125$°C, 28 min), the differences generated due to the single processes and the final transfer change can be seen in Figure 8B. The most pronounced changes occurred during hard baking. The largest height difference was observed at the structures' peak with a deformation of around 860 nm. This reflow effect has been already explained and modeled by [25]. A possible way to reduce reflow process is to hard bake the photoresist under vacuum [26] or UV hardening to increase the softening point of the photoresist [27], but these approaches were not tested in this work. Only slight differences were observed due to sputtering the plating base (thickness of 100 nm) and demolding. As the two latter steps show a positive change of height, they partially compensate the negative value of the first step, reducing the deformation created during hard baking to about 600 nm at the peak. As it was shown in Figure 6, the peak suffers such a large deformation that it can even be optically observed. This effect was observed after different hard baking processes. So, either higher temperatures or process durations can cause a non-uniform
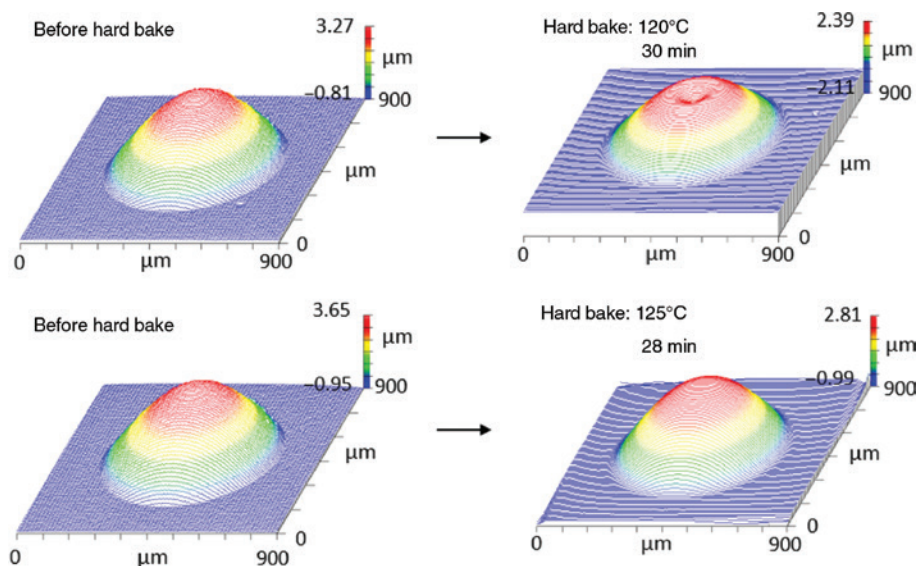
Figure 5: Patterned photoresist before and after hard baking in the oven, white light interferometer measurements.
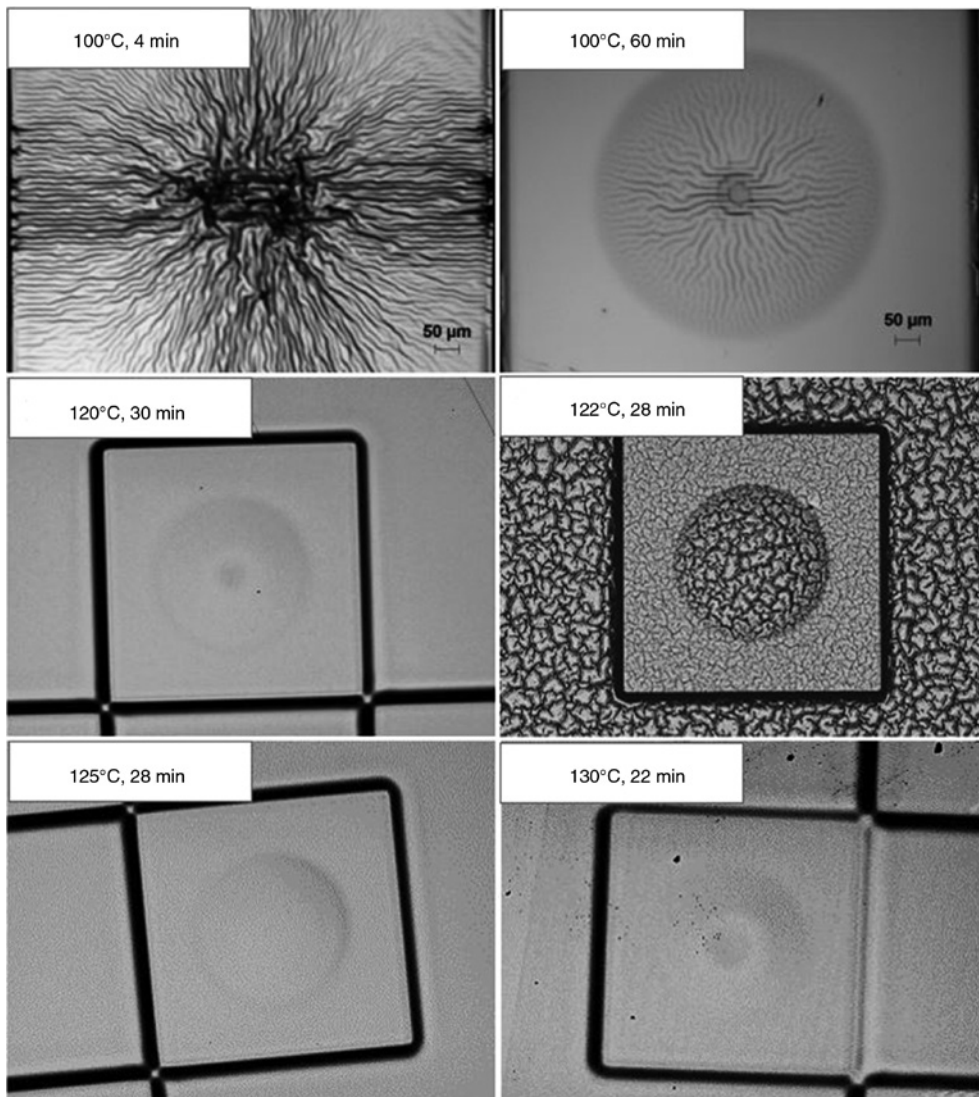
Figure 6: Sputtered samples after hard baking with different temperature values and process duration.
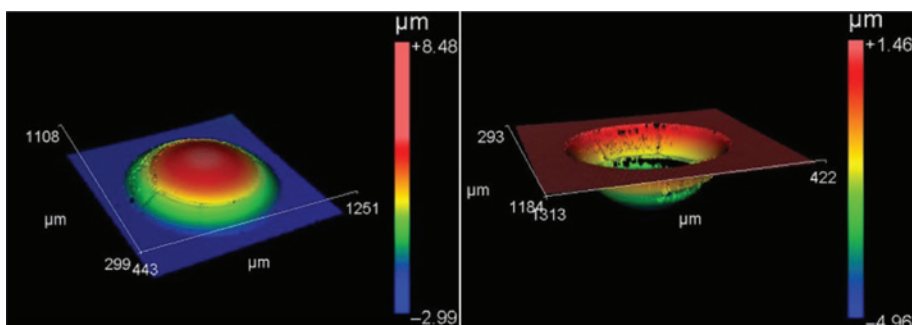
Figure 7: White light interferometer 3D plots: patterned photoresist (left image) and casted Cu after demolding from the photoresist (right image).

deformation. This was observed for both cases of non-appropriate process settings (see Figure 9), causing a large structure change. The largest variation was about 37% (1.45 µm) of the maximum height. Similar results as that for Cu microelectroplating were obtained for NiCo microelectroplating as shown in Figure 10A and B.
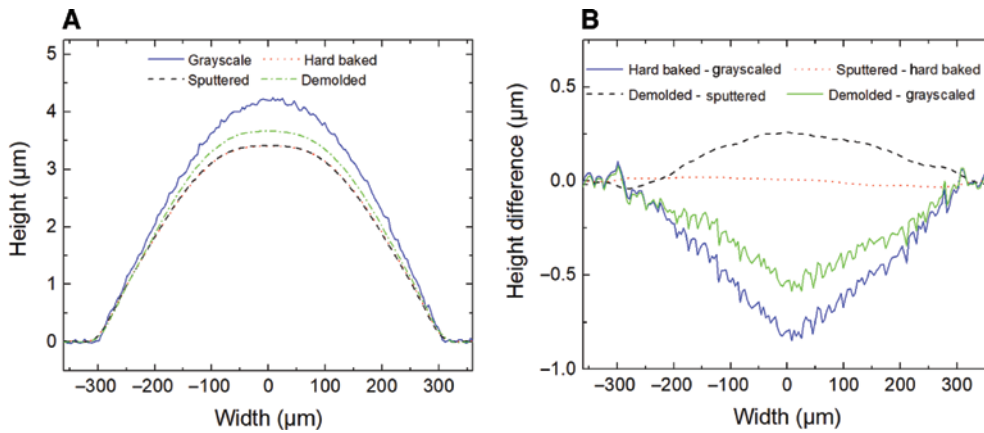
Figure 8: Cross section measurement from the 3D structure (A) after development, hard baking at a temperature of 125°C for 28 min (optimal hard bake conditions), sputtering, the final demolded sample Cu electrodeposited, and (B) the difference between these measurements.
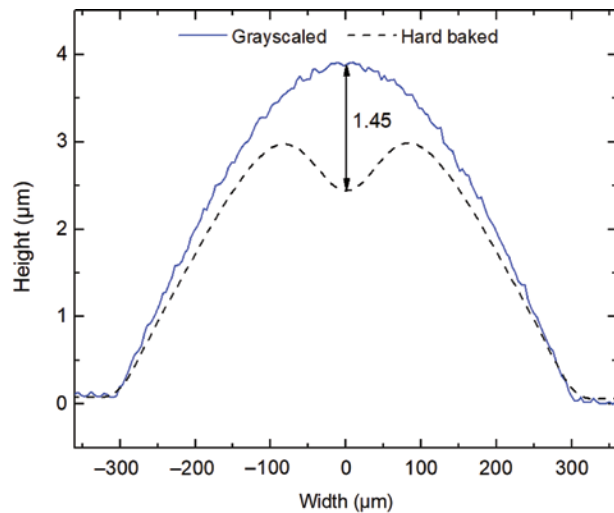
Figure 9: Photoresist deformation after hard baking at a temperature of 120°C for 30 min (non-optimal hard bake conditions).

The differences generated by every process step can be seen in Figure 10A, as well as the total difference. Once again, the most pronounced change occurred during hard baking, and the largest height deformation (around 680 nm) at the structure's peak. A difference of 180 nm was observed between the largest deformations from Figures 8B and 10B. The largest part of this deviation can be attributed to the grayscale exposure steps. Height difference fluctuations above 100 nm were observed when subtracting the exposure photoresist profile by the hard baked one. Moreover, process conditions and measurement misalignment can add up to this value. After microelectroplating, the difference has remained practically the same, showing the excellent pattern transformation of the microelectroplating process used. The following analysis was done taking a concave pattern under consideration. However, for the concave pattern, it was not possible to
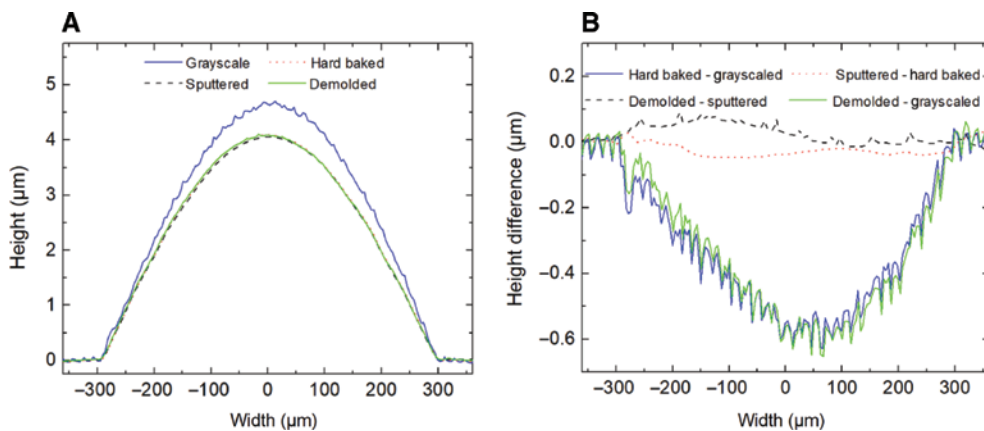
Figure 10: Cross section measurement from the 3D structure (A) after development, hard baking at 125°C for 28 min, sputtering, the final demolded NiCo electrodeposited sample, and (B) the difference between these measurements.

use a light interferometer due to the transparent properties of the photoresist and the shape under investigation. Therefore, a mechanical stylus profilometer was used with a scanning area of 1200 μm by 1200 μm. The measurement cross section after each process step is displayed in Figure 11A. Differently than the previous measurements, the reference for curve alignment was chosen to be at the bottom of the concave photoresist pattern (i.e. 0 μm in the *x* axis; see Figure 11A). This point has a photoresist thickness of roughly 1 μm, and it is assumed to suffer the lowest shrinkage during hard baking because it has the thinnest region. The photoresist's sharp corners became rounded, and a shrinkage of around 1 μm can be observed after hard baking. The largest deformations were observed at the sharp corners, and this can be clearly seen when displaying the difference between the measured curves (see Figure 11B). Very small changes can be noticed due to sputtering. However, this difference becomes even more pronounced (a total of around 1.9 μm) after microelectroplating due to the higher current density concentration incident at such corners. This effect could be reduced using techniques such as pulse plating.

4.2 Subtractive fabrication of 3D free forms

4.2.1 Photoresist structuring and pattern transfer by RIE

In comparison to the similar concept reported in [21], the concept of grayscale technology is further developed to fabricate an array of 3D microstructures into c-Si surfaces in this paper. The concept was implemented by the grayscale exposures of an array containing seven micropyramids with variable heights ranging from 2 to 8 μm

(interval of 1 μm), width of 74 μm, which are 10 μm apart. The height of the pyramids was defined with the respective gray values computed from the calibration curve (see Figure 2B) using Equation (1). Figure 12 shows the CAD mask design for the layout containing 8 square blocks, with each block containing 19 square frames, wherein the varying colors in each square block signify a specific square frame which belongs to a specific layer. The desired 3D micropyramid profiles were defined by assigning the respective gray values to each individual layer. The CAD mask layout from Figure 12 was exposed, developed, hard baked and characterized to measure the resultant dimensions and 3D profile using an optical microscope, a profilometer and an SEM, respectively. Furthermore, considering the optimized hard bake conditions obtained in Section 4.1, the developed 3D micropyramids were hard baked in oven for 115°C for 60 min. Again, the hard baking condition was found to have a profound influence on the 3D micropyramid profile geometry, wherein the structure height decreased. The 3D micropyramids after the hard bake were etched in RIE with optimized process conditions as mentioned in Section 2. The RIE etching time was set corresponding to the highest thickness of the 3D pyramid (i.e. 8 μm in this study).

4.2.2 Transfer characterization

Figure 13A–C shows the SEM micrographs of the 3D micropyramids in the photoresist after development, after hard bake and after transfer into c-Si, respectively. The steps of the gray values corresponding to the 19 square frames in the CAD mask layout design as shown in Figure 12 can be seen in Figure 13A. However, the transition in the
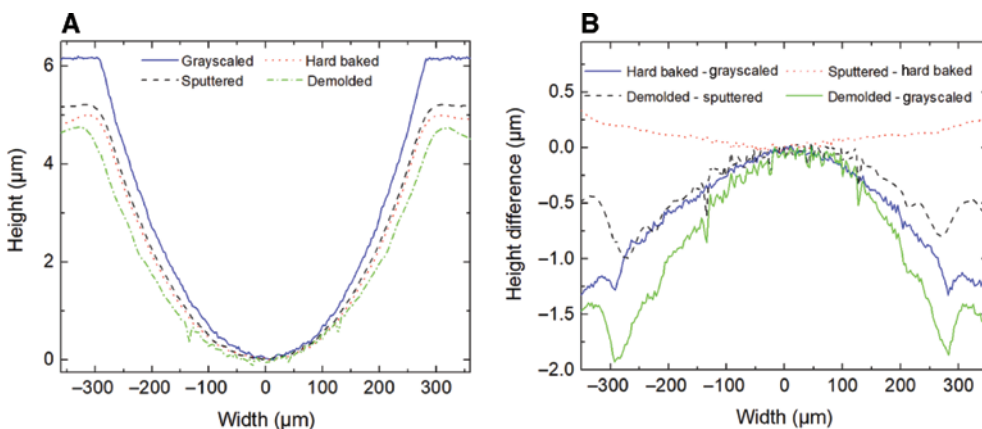
Figure 11: Cross section (A) measurement of the concave pattern after development, hard baking, sputtering, the final demolded Cu electrodeposited sample, and (B) the difference between these measurements.
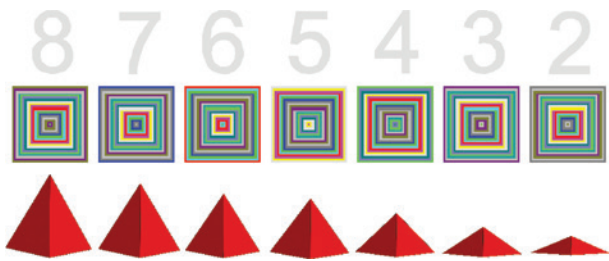
Figure 12: CAD mask design to expose 3D micropyramids with different heights using grayscale lithography, each block contains 19 designs and is 74 μm².

micropyramid shows a step that can be attributed when two adjacent layers were allotted to a same gray value, which can be optimized by coding the gray values to the corresponding layers in the DWL 66FS CAD conversion software. Furthermore, the 3D micropyramid undergoes a very significant reflow during the hard baking step in the oven, wherein the structure geometry and the dimension are found to be profoundly affected as shown in Figure 13B. The surface of the 3D micropyramids is found to be more smoothened without sharp edges in contrast
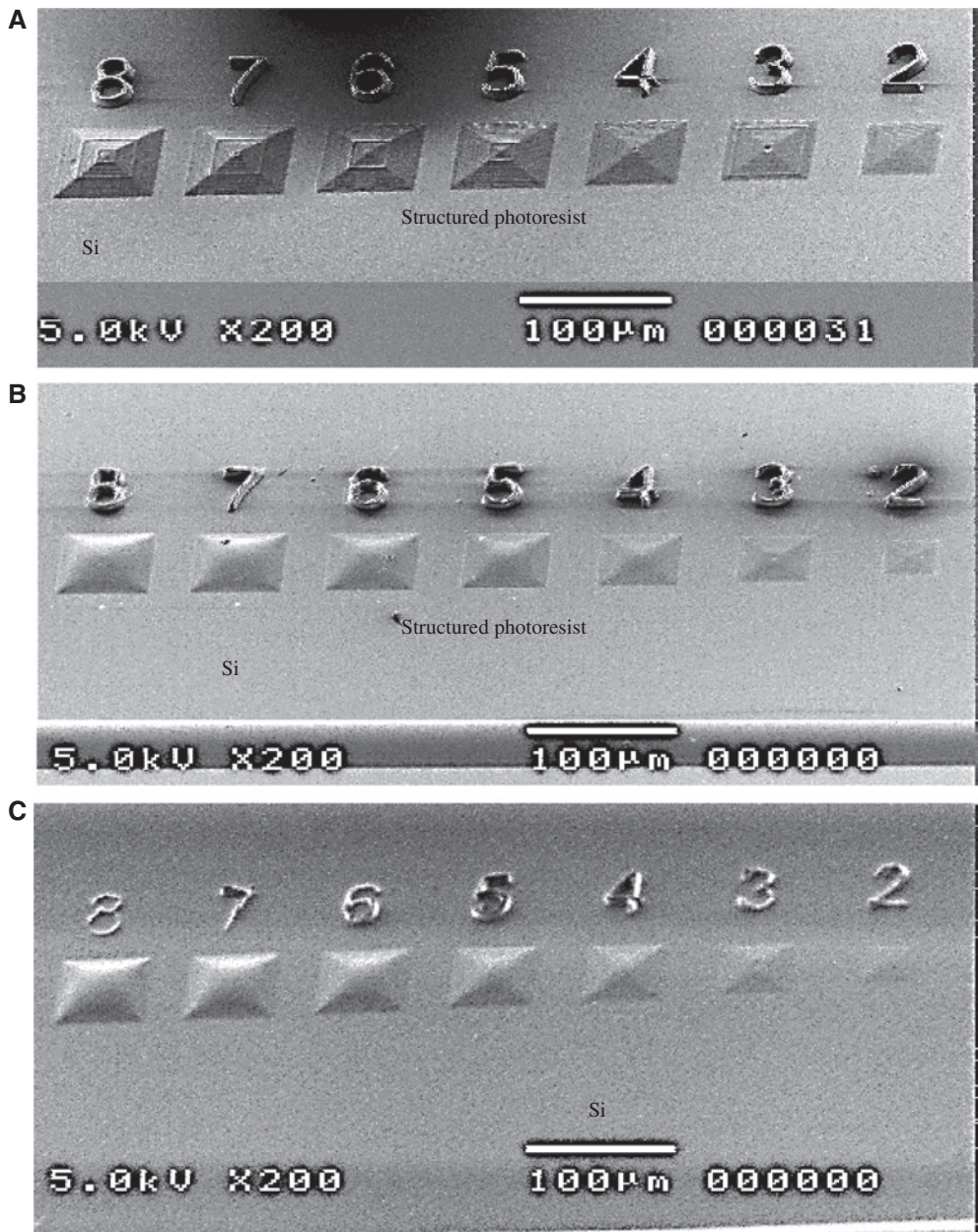
Figure 13: 3D micropyramids with variable heights 2–8 μm (A) exposed in AZ4562 by grayscale lithography by DWL before hardbake (B) after hardbake and (C) 3D micropyramids transferred into c-Si.

to Figure 13A. The influence of the reflow process on the structure dimension is measured using the profilometer as shown in Figure 15. The peak corresponding to the 3D micropyramid with 8-μm height (CAD) shows effectively about 8.5 μm in measurement because of the sharp peak of the pyramid that spikes up the height profile in the measurement as the profilometer tip traverses the peak region, which is also the case for other 3D micropyramids. However, this effect is not so prominent for shorter-height 3D micropyramids. The reduction in the height of the 3D micropyramids as a result of the hard bake can be clearly seen in the profilometer measurements in Figure 15. The height reduction during the hard bake (which heats up the photoresist) is due to the reflow process, thereby changing the geometric profile of the 3D structures. Moreover, the reflow process is more prominent in the case of the 3D

micropyramids, which have steep side walls and a sharp peak compared to the convex and concave structures as shown in Section 4.1. This effect can be attributed to the higher energy gradients between the micropyramid peak and the base as compared to similar-height convex/concave structures; the reflow process in polymers is modeled and comprehensively elucidated by Kirchner et al. [28, 29], where the authors explain the mechanism behind the polymer reflow process. Therefore, similar to the additive process reported in Section 4.1, hard baking of the structured photoresist is a critical process for grayscale technology, as it has been previously reported [21] that the hard bake with a hotplate served as better approach than the oven for the subtractive fabrication using RIE. The postbake time (1 min) and temperature (80°C) were significantly smaller with the hotplate as compared to the oven, thereby preventing the reflow of the photoresist.

The 3D micropyramids after the hard bake were etched in RIE using the optimized process conditions [19] to attain 1:1 selectivity, and Figure 13C shows the SEM micrographs of the transferred pattern in the c-Si. The pattern transfer in the c-Si is a replica of the pattern in the Figure 13B. The 3D profile measurement of the 3D micropyramids after the hard bake and after the RIE is shown in Figure 14A and B, respectively. Furthermore, Figure 15 shows the dimensional comparison of the 3D micropyramids after the hard bake and the pattern in the c-Si after transfer for the optimized process settings. It can be seen that the structure height, the width and the 3D profile are well preserved during the final pattern transfer, and the 3D micropyramids are transferred with high accuracy into the c-Si. Additionally, the surface roughness of the c-Si after RIE etching was measured using AFM, wherein the arithmetic average roughness value, which were calculated from areas of 5 and 2 μm^2, was 4.6 and 4 nm, respectively. The resultant average roughness values are about 10 times larger than those of a polished c-Si wafer, however smooth enough to enable the fabrication of 3D optical microcomponents using this approach.
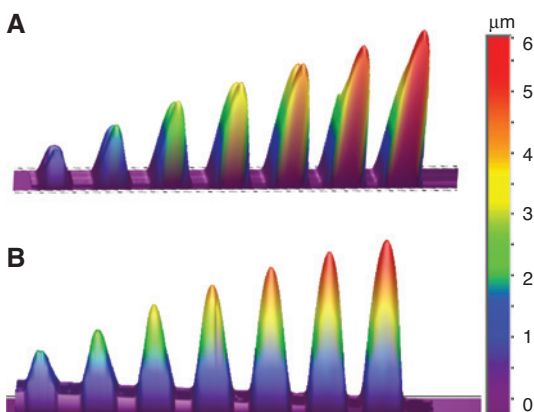
Figure 14: Measured profile of the 3D micropyramids using a Dektak profilometer (A) in photoresist in AZ4562 after hard bake and (B) in Si after RIE 1:1 transfer.
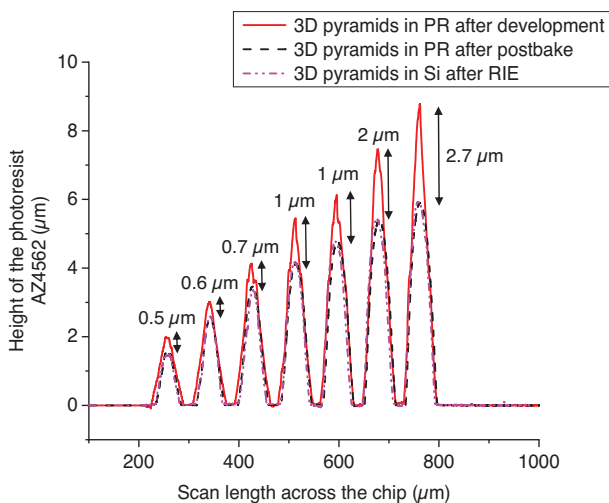
Figure 15: Comparison of the 3D micropyramid height in photoresist (before etching), after hard bake and Si (after RIE).

5 Conclusions

Complete processes were developed to produce 3D microstructures using additive and subtractive pattern transfer methods. Grayscale lithography is combined with micro-electroplating for additive fabrication of 3D free forms in Cu and NiCo alloys. Furthermore, it is combined with RIE for 1:1 pattern transfer by the subtractive method into c-Si using optimized process conditions to attain

a selectivity = 1 and an anisotropy factor close to 1. 3D convex lens-like structures were exposed in AZ4562 positive photoresist and used for additive fabrication, thereby resulting in concave replicas in Cu and NiCo, respectively. As a proof of concept, an array of 3D pyramids with variable heights was exposed in AZ4562 positive photoresist and used for subtractive fabrication by RIE into the c-Si. Exact replicas of the 3D patterned photoresist can be obtained in c-Si using subtractive fabrication, while negative replicas can be obtained in metals and alloys using the additive fabrication method. The hard bake condition is found to be a very crucial step in both the additive and subtractive fabrication; for the former case, it influences significantly the adhesion of the seed layer, and in the latter case, it significantly affects the 3D profile geometry and the dimensions of the 3D microstructures. Using both the additive and subtractive fabrication processes, the pattern transfer can be attained with high accuracy. The main drawback of this process is a narrow process window to maintain a quasi-perfect structure and to avoid both crack formation and wrinkled surfaces during hard baking of the used positive photoresist. Results of hard baking using different parameters are shown during this work, as well as their optimization. Furthermore, a compensation for the designed structures or the use of different photoresists such as the negative working SU-8 might be required depending on the accuracy required by the final application. This process is an efficient tool for hot embossing, molding and imprinting, as well as for direct functional structuring in silicon microsystems.

References

[1]   E. W. Becker, W. Ehrfeld, P. Hagmann, A. Maner and D. Münch-meyer, Microelectron. Eng. 4, 35–56 (1986).

[2]   R. Bischofberger, H. Zimmermann and G. Staufert, Sens. Actuators A Phys. 61, 392–399 (1997).

[3]   H. Schift, Appl. Phys. A 121, 415–435 (2015).

[4]   Y. Lu and S. Chen, Appl. Phys. Lett. 92, 41109 (2008).

[5]   Z. D. Popovic, R. A. Sprague and G. A. Connell, Appl. Opt. 27, 1281–1284 (1988).

[6]   T. Bourouina, T. Masuzawa and H. Fujita, J. Microelectromech. Syst. 13, 190–199 (2004).

[7]   Z. Peng, D. Fattal, A. Faraon, M. Fiorentino, J. Li, et al., Opt. Lett. 36, 1515–1517 (2011).

[8]   J. P. Marsh, D. J. Mar and D. T. Jaffe, in 'Ground-based and Airborne Instrumentation for Astronomy', Eds. By I. S. McLean, M. Iye, vol. 6269, (Proc. SPIE, 2006) p. 62694J.

[9]   G. Yoo, H. Lee, D. Radtke, M. Stumpf, U. Zeitner, et al., Microelectron. Eng. 87, 83–87 (2010).

[10] S. Jeon, V. Malyarchuk, J. O. White and J. A. Rogers, Nano Lett. 5, 1351–1356 (2005).

[11] D. Therriault, S. R. White and J. A. Lewis, Nat. Mater. 2, 265–271 (2003).

[12] J. K. Gansel, M. Thiel, M. S. Rill, M. Decker, K. Bade, et al., Science (New York, NY) 325, 1513–1515 (2009).

[13] C. Stilson, R. Pal and R. A. Coutu, in M. A. Maher, P. J. Resnick (Eds.), Micromachining and microfabrication process technology XIX, SPIE, 2014, 89730E.

[14] A. Schaap and Y. Bellouard, Opt. Mater. Express 3, 1428 (2013).

[15] S. Diez, in 'Emerging digital micromirror device based systems and applications VIII' Eds. by M. R. Douglass, P. S. King, B. L. Lee (SPIE, 2016) p. 976102.

[16] Y.-H. Hung, H.-L. Chien and Y.-C. Lee, Appl. Sci. 8, 1690 (2018).

[17] C.-C. Chiu and Y.-C. Lee, Int. J. Mach. Tool. Manu. 70, 15–21 (2013).

[18] J. K. Tseng, Y. J. Chen, C. T. Pan, T. T. Wu and M. H. Chung, Solar Energy 85, 2167–2178 (2011).

[19] Heidelberg Instruments Mikrotechnik GmbH, Device Specification, The DWL 66FS laser lithography system, Heidelberg, Germany (2008).

[20] U. M. Isman Khazi, Self-aligning micro punch-die tool-system for high precision blanking of thin metal foils (Mikrosystemtechnik Kongress, Karlsruhe, 2015).

[21] I. Khazi, U. Muthiah and U. Mescheder, Microelectron. Eng. 193, 34–40 (2018).

[22] E. Kieselstein, J.-P. Sommer, K. Brämer, V. Großer, W. Benecke, et al., Microsyst. Technol. 7, 196–202 (2001).

[23] S. Audran, B. Faure, B. Mortini, J. Regolini, G. Schlatter, et al., Microelectron. Eng. 83, 1087–1090 (2006).

[24] S. Audran, B. Mortini, B. Faure and G. Schlatter, J. Micromech. Microeng. 20, 95008 (2010).

[25] F. T. O'Neill and J. T. Sheridan, Optik 113, 391–404 (2002).

[26] S. B. Matthias Heschel, Sens. Actuators A 70, 75–80 (1998).

[27] R. Allen, J. Electrochem. Soc. 129, 1379 (1982).

[28] R. Kirchner, A. Schleunitz and H. Schift, J. Micromech. Microeng. 24, 55010 (2014).

[29] R. Kirchner and H. Schift, Mater. Sci. Semicond. Process. 92 58–72 (2019).